ACS Photonics

Article

pubs.acs.org/journal/apchd5

Ceramic Photonic Glass for Broadband Omnidirectional Reflection

Pavel N. Dyachenko,*[,†] Jefferson J. do Rosário,[‡,§] Elisabeth W. Leib,[‡,∥] Alexander Yu. Petrov,[†,⊥] Roman Kubrin,[§] Gerold A. Schneider,[§] Horst Weller,[∥,#] Tobias Vossmeyer,[∥] and Manfred Eich[†]

[†]Institute of Optical and Electronic Materials, Hamburg University of Technology, Eissendorfer Strasse 38, 21073 Hamburg, Germany

[§]Institute of Advanced Ceramics, Hamburg University of Technology, Denickestrasse 15, 21073 Hamburg, Germany

[∥]Institute of Physical Chemistry, University of Hamburg, Grindelallee 117, 20146 Hamburg, Germany

[⊥]ITMO University, 49 Kronverskii Ave., 197101, St. Petersburg, Russia

[#]Department of Chemistry, Faculty of Science, King Abdulaziz University, Jeddah, Saudi Arabia

ABSTRACT: We report on the fabrication and properties of ceramic photonic glass, a disordered arrangement of monodisperse ceramic spheres with diameters in the range of the wavelengths of incident light. These novel materials are produced as solid thin films which can be used for a wide range of applications, such as broadband visible reflectors, thermal radiation barrier coatings, high temperature stable structural coloration, resonant random lasers and media for photonic Anderson localization. Large nearly monodisperse spheres of different sizes were obtained by methods of sol−gel chemistry. Photonic glass films with layer thickness varied in the range 7−100 μm were deposited by drop casting from suspensions in ethylene glycol. Larger particles demonstrate a larger spectral window of broadband reflection. For thermal barrier coating applications strong reflection in the wavelength range of 1−6 μm is obtained with particles close to 3 μm diameter.

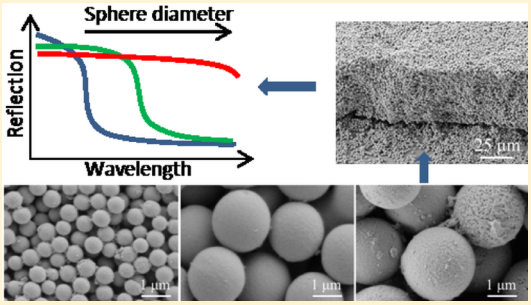

KEYWORDS: *broadband reflection, zirconia microspheres, monodisperse ceramic particles, photonic glass, Mie resonances*

Multiple scattering of light in a random media is a subject of great interest in fundamental and applied photonics research.[1,2] Applications can be found in the reflective coatings industry,[3] imaging,[4,5] structural coloration,[6] and thermal barrier coatings.[7,8] Moreover, a number of interesting physical phenomena, such as coherent light backscattering,[9] random lasing,[10] and strong light localization[11] have arisen from the study of such systems. García et al.[12,13] presented a new three-dimensional system, called a photonic glass, that is composed of monodisperse polymer spheres arranged in a completely disordered way. Due to the resonant behavior of the spheres, discrete light states exist, and therefore, every sphere acts as a meta-atom for light. Active photonic glasses can be used to create random lasing materials and to tune the lasing emission wavelength.[14] A high refractive index contrast of the dielectric in air provides strong scattering effects and the Mie resonances have spectral selectivity. Both open up new ways toward active disorder-based photonic devices.

A strong scattering of light in the disordered structure and the resulting high diffuse reflectance over a broad wavelength range make photonic glasses also attractive for other fields of science and technology. For reflective coatings it is important to minimize the layer thickness while maintaining a strong reflection, as it is desirable to minimize both weight increase and the use of often costly materials. For example, thermal barrier coatings (TBCs) should combine a low thermal conductivity as observed in porous ceramics with a strong reflection of thermal radiation for the wavelength range from 1 to 6 μm.[8] The broadband reflection of electromagnetic radiation could be realized if several photonic structures with different spectral locations of the photonic band gaps would be stacked upon each other. Kelly et al. have studied a broadband reflection of a one-dimensional layered system consisting of yttrium-stabilized zirconia and alumina alternating layers of variable thickness.[15] Due to the small width of the band gap of such a 1D-Bragg-stack such a layered system shows an increased reflection in the wavelength range from only 1 to 2.75 μm. Responsible for this is the relatively low dielectric contrast between two adjacent layers which, compared to concepts that employ larger index contrasts, also increases the number of layers required for a certain reflectivity. The concept of TBCs based on 3D multistack photonic crystals was presented recently.[16,17] Simulations have shown that the full coverage of the blackbody radiation spectrum for the wavelength range from 1 to 5 μm require 10 stacks of inverse opals with different lattice constants. Even employing a larger refractive index contrast due to the air pores the reflection bands of the photonic crystals remain comparatively narrow. Lee et al. have experimentally demonstrated that two layers of titania inverse opal with different pore sizes can possess two distinctive photonic stop gaps over a broad angle range.[18]

Received: June 19, 2014
Published: September 30, 2014

However, due to a multistep fabrication process, these multistack photonic crystals possess various types of defects such as point/line defects, stacking faults and cracks.[18,19] Hence, the reflection efficiency of such systems is decreased. Therefore, alternative approaches for realization of the broadband reflectors of the thermal radiation should be pursued. Particularly interesting are systems implying less involved fabrication route and less affected by defects. Concerning these both issues, disordered systems have an obvious advantage over the photonic crystals as they essentially do not require a high degree of perfection.

In this work, we present a new material ceramic photonic glass. This three-dimensional system is composed of monodisperse zirconia spheres arranged in a disordered way. We used zirconia spheres for fabrication of photonic glass. Widoniak et al.[20] reported on the fabrication of zirconia particles in a size range from 0.2 to 2 μm with standard deviations between 10 and 15%. In general, the main problem in synthesizing monodisperse particles, that is, particles with a size distribution below 10%, resides in the occurrence of secondary nucleation and agglomeration of particles. Yan et al.[21] managed to fabricate larger particles with diameters ranging from 0.8 to 3.6 μm. However, the corresponding standard deviations were between 6 and 37%. Here, the main challenges involve the synthesis of particles with very narrow size distributions and smooth surfaces in the cases of smaller diameters and avoiding secondary nucleation and agglomeration, especially in the case of larger particles. We were able to synthesize zirconia microparticles with sizes ranging from 0.7 to 2.6 μm (after heat treatment at 450 °C) and consistently low standard distributions from 5 to 10%. These monodisperse ceramic spheres were assembled into crack-free disordered photonic layers with thicknesses ranging from 7 to 100 μm. Reflectivity measurements on these layers showed a broadband reflection in the infrared which was in good agreement with our theoretical calculations.

Such ceramic photonic glasses could be used as next-generation TBCs that would not only reduce heat transfer by thermal conduction but also effectively reflect thermal radiation employing small layer thicknesses. As we show the disordered structures offer the advantage of broadband reflectance which could eliminate the need for depositing multilayer coatings. At the same time, such disordered structures offer the potential of very low thermal conduction due to the limited contact areas between single spheres. Due to their large index contrast ceramic photonic glasses are also highly interesting media for the investigation of resonant random media properties, such as random lasing and photonic Anderson localization. One additional interesting optical property of photonic glasses is the feature of noniridescent structural coloration.[6,22−24] Our ceramic photonic glasses have high refractive index contrast of ceramic and good monodispersity of particles. Thus, they demonstrate pronounced Mie resonances that can be also used as structural coloration. Standard inorganic pigments are still widely used to color materials exposed to elevated temperatures during processing or application.[25] However, most inorganic pigments contain heavy metals that can adversely influence on the environment and human health.[26] High temperature stable coloration ceramic materials without any pigments based on heavy metals or transition metals can be used as an ecologically friendly alternative.

RESULTS AND DISCUSSION

Structure and properties of three-dimensional arrays of ZrO_2 ceramic microparticles with particle diameter D (see inset in Figure 1) and layer thickness L were investigated. The

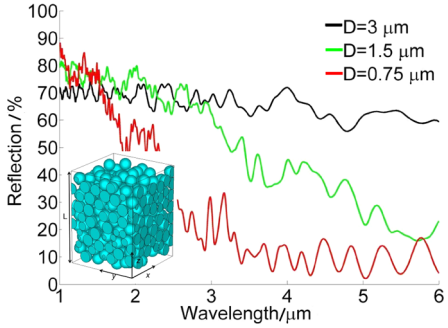

Figure 1. Calculated hemispherical diffuse reflection from disordered photonic structures with sphere diameter D = 0.75, 1.5, and 3 μm and thicknesses L = 18 μm. The inset shows the schematic of the disordered photonic structure.

hemispherical diffuse reflection of such a system can be obtained by $R = 1 - T$, where R is the hemispherical diffuse reflection and T is the hemispherical diffuse transmission, assuming low absorptivity of ZrO_2 for wavelengths in the visible and NIR range.[15]

The results of the calculations are shown in Figure 1 for D = 0.75, 1.5, and 3 μm at constant film thickness of 18 μm. It can be observed from Figure 1 that the larger particles demonstrate a larger bandwidth of reflection. At large wavelengths, when the wavelength is much larger than the particle size, all structures become transparent. The reflection efficiency in the reflection window also depends on the diameter of the microparticles. Smaller particles have smaller spectral window of reflection but at the same time stronger reflection in this window. The particles with diameter smaller as 1 μm can efficiently reflect visible and NIR radiation. To cover all spectral range from 1 to 6 μm it turns out that one should use particles close to 3 μm diameter.

The hemispherical diffuse transmission of a random system is expressed by the photonic Ohm's law which states that the total transmission is proportional to the ratio of the transport mean free path $l_t(\lambda)$ (the average distance over which the scattered light direction is randomized), to the thickness of sample L: $T \sim l_t(\lambda)/L$.[27] The necessary condition for the validity of the photonic Ohm's law is that $l_t(\lambda) \ll L$, which means that the light has been multiply scattered in the material before exiting. In order to obtain a reflector with maximized reflectance in a broad spectrum range for minimal thickness, the figure of merit function F, which characterizes the reflectance performance independent of the thickness, needs to be analyzed for each particle size used. The figure of merit function F is described as follows:

$$F = \frac{1}{T_{av}L} = \frac{1}{(1 - R_{av})L} \quad (1)$$

where

$$T_{av} = \frac{1}{\lambda_2 - \lambda_1}\int_{\lambda_1}^{\lambda_2} T(\lambda)\mathrm{d}\lambda \quad (2)$$

dx.doi.org/10.1021/ph500224r | ACS Photonics 2014, 1, 1127−1133

is the transmission averaged over the spectral range, $R_{av} = 1 - T_{av}$ is the averaged hemispherical diffuse reflection (for nonabsorptive materials), (λ_1,λ_2) denotes the wavelength range. Corresponding to the photonic Ohm's law our figure of merit F is independent of the thickness of the sample. It means F is only a function of geometrical parameters of the sample's constituents (size, shape of particles, and filling fraction) and the refractive index.

For 3 μm spheres further results are shown in Figure 2 for L = 14, 32, 50, and 81 μm. The calculated figure of merit F for the

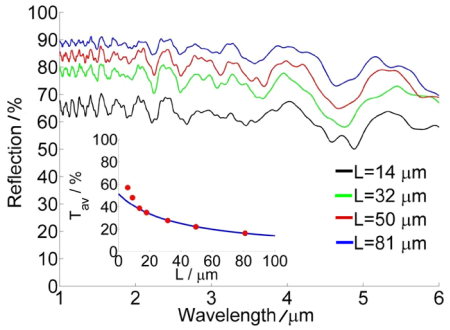

Figure 2. Calculated hemispherical diffuse reflection from disordered photonic structures with sphere diameter D = 3 μm and different thicknesses. The inset shows the average transmission as a function of layer thickness. The red points are simulation results; the blue line is a fit by photonic Ohm's law.

wavelength range (1−6 μm) for the disordered array of ZrO_2 microparticles with 3 μm diameter is equal to 0.058 μm^{-1}. The inset in Figure 2 shows the average transmission as a function of the layer thickness. In accordance with the photonic Ohm's law the average hemispherical diffuse transmission T_{av} for thickness $L \gg l_t(\lambda)$ can be fitted to a hyperbola. It can be seen that the calculated results can be described by Ohm's law for L > 15 μm.

Monodisperse zirconia particles with a diameter of 0.67 μm were fabricated by a modified sol−gel approach according to the Widoniak method.[20] The main problem related to the synthesis of monodisperse particles using the approach reported by Widoniak et al. was the occurrence of secondary nucleation and agglomeration. This could be avoided by adjusting some critical parameters, such as the use of fatty acids as stabilizers, continued stirring during the aging time and cold centrifugation. This modified process lead to reproducibly monodisperse particles with virtually no agglomeration and secondary nucleation. Zirconia particles with diameters of 2.1 and 2.6 μm were synthesized using a modified version of the Yan method.[21] The synthesis performed according to the method of Yan et al. was modified by adapting the aging parameters (temperature, rotation speed, and aging time) and the work up (cold centrifugation). The particles yielded this way exhibited a smooth surface and both a low degree of both agglomeration and secondary nucleation. The particles were spherical with a smooth surface. Particles sizes were measured with SEM images from 200 particles per batch. Average sizes and standard deviations achieved were 0.67 μm ± 4.9%, 2.1 μm ± 8.8%, and 2.6 μm ± 7.3%. Size distribution histograms are shown in Figure 3.

Figure 4 shows XRD spectra from one example of particles without calcination (after synthesis) and after calcination of the layers at 600 °C (D = 0.67 and 2.1 μm) and 700 °C (D = 2.6

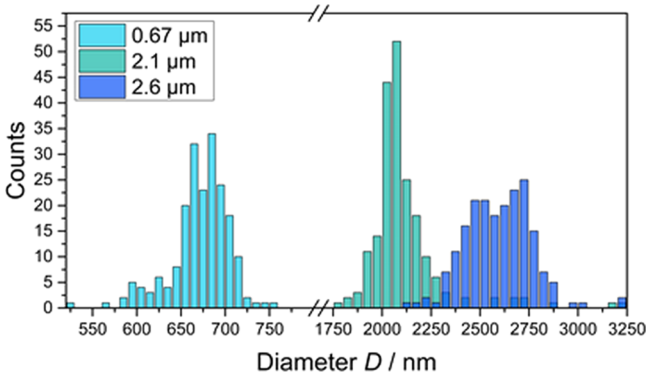

Figure 3. Size distribution histograms for the three particle samples used for assembly.

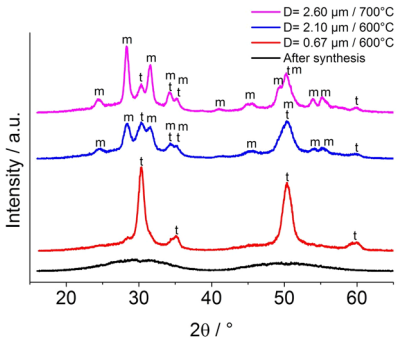

Figure 4. XRD spectra of layers deposited from the zirconia microspheres. Layers from particles with D = 0.67 μm calcined at 600 °C present a tetragonal phase, with D = 2.10 μm calcined at 600 °C and D = 2.6 μm calcined at 700 °C a mixture of tetragonal and monoclinic phases. Tetragonal phase (t) corresponding to JCPDS 42−1164 and monoclinic phase (m) to JCPDS 37−1484. A spectrum from particles after synthesis is also given as comparison. The particles are amorphous in the as synthesized state.

μm). As synthesized particles are amorphous. Particles with D = 0.67 μm calcined at 600 °C are in the tetragonal phase (JCPDS 42−1164). Particles with D = 2.1 μm calcined at the same temperature present a mixture of tetragonal and monoclinic (JCPDS 37−1484) phases. This difference in crystalline structure is presumably due to difference in the size of the particles and due to starting precursors. Similarly, particles with D = 2.6 μm present a mixture of tetragonal and monoclinic phases, with an increase in the amount of monoclinic phase compared to particles with D = 2.1 μm.

The microstructures of the layers were observed and their thickness measured by scanning electronic microscope. Figure 5 shows higher and lower magnification of the surface and cross-section (tilted 45°) of the deposited photonic glasses from spheres with diameters of (a, d, g) 0.67 μm, (b, e, h) 2.1 μm, and (c, f, i) 2.6 μm. With higher magnification of the surface (Figure 5a−c) the spherical shape and the rather smooth surface of the building blocks can be observed, also small particulates are visible. Small nonspherical particulates, which were not present in the as-synthesize particles, are a result of the sonication used to redisperse the precalcined particles in ethylene glycol. Lower magnification images (Figure 5d−f) show that large area crack-free layers were achieved, thus leaving no free path for incident radiation. Figure 5g−i shows the cross-section of the layers with (g) 10, (h) 45, and (i) 80 μm thicknesses.

dx.doi.org/10.1021/ph500224r | ACS Photonics 2014, 1, 1127−1133

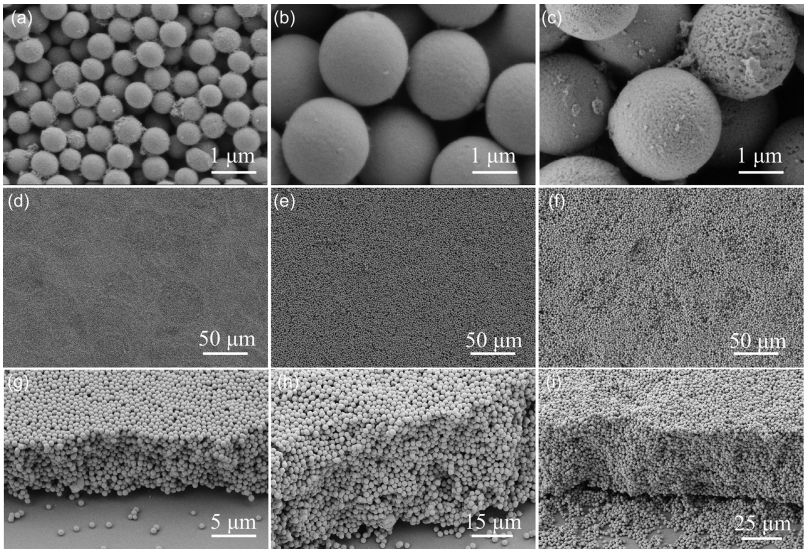

Figure 5. SEM images of photonic glasses deposited from spheres with diameters of (a, d, g) 0.67 μm, (b, e, h) 2.1 μm, and (c, f, i) 2.6 μm. Images correspond to the surface at higher and lower magnification and cross-section (tilted 45°). The samples have (g) 10, (h) 45, and (i) 80 μm thicknesses.

We observed no ordering in the deposited films. The photonic glass formation and the absence of crystallization in a system of hard spheres are usually associated with a high polydispersity. The diameter and the density of spheres have a large influence on the self-assembly. Heavy particles are not stable in suspensions and sediment very fast. This leads to a random packing of the spheres in the obtained particulate films.

Figure 6 presents the hemispherical diffuse reflectance spectra for samples with the diameters 0.67, 2.1, and 2.6 μm. It can be observed from Figure 6 that the spectral reflectance increases with the thickness and decreases with increasing wavelength. These trends are observed both in simulations as well as in the measurements. Increasing the diameter of microparticles can improve the reflectance of photonic glasses for a more broadband spectrum. The reflectance dip at wavelengths of 3.0−4.5 μm is due to the OH groups incorporated at the ZrO_2 microparticles' surface and due to H_2O absorption, which is expected to disappear at TBC working temperature, so they will not play an active role in the reflection and absorption of the coatings. The reflectance dip at wavelengths of 4.2 μm is corresponding to CO_2 absorption from the exterior atmosphere. The inset in Figure 6 (c) presents the reflection of the ceramic photonic glasses (D = 2.6 μm and L = 100 μm) for both an unannealed sample and the sample annealed at T = 900 °C for 1 h. It can be seen that for TBC working temperature the reflectance dip at wavelengths of 3−4.5 μm is significantly reduced. The atmospheric CO_2-absorption peak at 4.2 μm is still present.

The photonic glass with D = 2.1 μm microparticles can be used for efficient reflection in the range from 1 to 2.5 μm for room-temperature applications. Moreover, the photonic glass with particles smaller than 1 μm is also beneficial for efficient reflection in visible range (see below, Figure 7). As shown in Figure 6c, the reflectance of photonic glass with D = 2.6 μm microparticles is high at wavelengths ranging from 1 to 6 μm, indicating that the photonic glass is a strong scattering material at the wavelength where thermal radiation inside turbine engines at operating temperatures is most concentrated. This is beneficial for the TBC applications because most of the incident radiation will be reflected back to the hot gas stream instead of being absorbed by the coating. At a given cooling rate of the cooling system this reflection will thus limit the steady state temperature in the superalloy based turbine blades. The figure of merit function F for the measured wavelength range 1−6 μm for sample with D = 2.6 μm microparticles is equal to 0.037 μm^{-1}. The averaged reflection for sample with L = 100 μm is equal to 73%. To obtain the same reflectance by suspension plasma-sprayed yttrium-stabilized zirconia, a 370 μm thick layer is needed.[28]

At the same time, disordered structures offer the potential of very low solid heat conduction due to the limited contact areas between single microspheres. An effective solid thermal conductivity of the ceramic photonic glass can be calculated by the model proposed in work by Gusarov and Kovalev.[29] The effective thermal conductivity of the ceramic photonic glass λ_e is expressed as

$$\frac{\lambda_e}{\lambda_s} = \frac{fNd}{\pi D} \tag{3}$$

where d is the diameter of the contact size between spheres, D is the diameter of the sphere, N is the coordination number of the sphere (a number of nearest neighbors), f is the material filling fraction, and λ_S is the solid thermal conductivity of material. The mean coordination number of photonic glass with f = 0.5 is equal to N = 6.[29] If we assume the realistic parameters of ZrO_2 solid thermal conductivity λ_S = 2 W/mK and the diameter of contact size between spheres d = 200 nm, we have the effective thermal conductivity λ_e = 0.14 W/mK for microspheres with D = 2.6 μm. This value is significantly smaller than the thermal conductivity of suspension plasma-sprayed YSZ of 0.5−1 W/mK.[30]

To compare the effects of thermal conductance and radiation heat transfer we estimate transferred powers by both mechanisms in a typical high temperature environment. The heat flux transferred through a layer of ceramic photonic glass with thickness L = 100 μm by conduction can be estimated as $Q_{con} = \lambda_e \Delta T/L$, where ΔT is the temperature gradient between hot and cold interfaces. If we assume the realistic value of ΔT = 200 °C,[32] we have the heat flux Q_{con} = 28 W/cm^2. For the

dx.doi.org/10.1021/ph500224r | ACS Photonics 2014, 1, 1127−1133

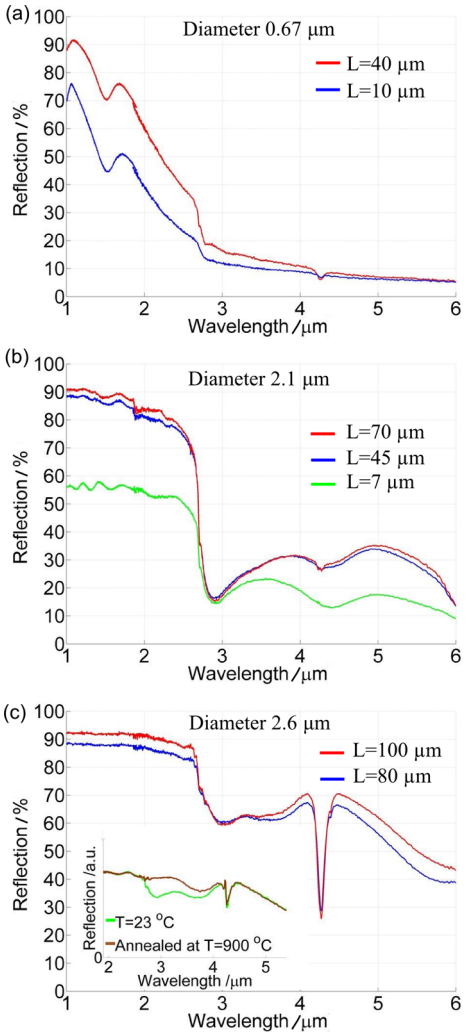

Figure 6. Experimental hemispherical diffuse reflection from ceramic photonic glasses with sphere diameter D = 0.67 μm (a), D = 2.1 μm (b), and D = 2.6 μm (c). Insertion in (c) shows experimental reflection from ceramic photonic glasses for T = 23 °C and T = 900 °C for the sample with a sphere diameter D = 2.6 μm and L = 100 μm.

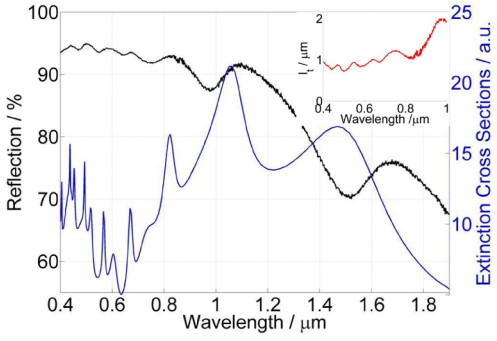

Figure 7. Experimental hemispherical diffuse reflection from ceramic photonic glass with sphere diameter D = 0.67 μm (L = 40 μm) and extinction cross section for single sphere of the same diameter. The partial disagreement between experimental and theoretical data for resonances at long wavelengths comes from interaction between the particles. Insertion shows the experimental transport mean free path in a photonic glass with sphere diameter D = 0.67 μm.

calculation of the heat flux transferred by radiation, we assume an environment of hot gas as a blackbody emitter with temperature Tm_g = 1500 °C. For thickness L = 100 μm the heat flux transferred by radiation can be estimated as $Q_{rad} \approx T_{av}\sigma Tm_g^4$, where T_{av} is the averaged hemispherical transmission for the range 1−6 μm and σ is the Stefan−Boltzmann constant. For our ceramic photonic glass with D = 2.6 μm and L = 100 μm we have T_{av} = 0.27 and Q_{rad} = 15 W/cm^2. Thus, both heat fluxes are comparable and sum up to $Q_{tot} = Q_{con} + Q_{rad}$ = 43 W/cm^2. For a relatively thin coating of 100 μm this is an order of magnitude smaller heat flux compared to conventional TBCs[30] if a realistic value for the thermal conductivity is assumed.

Photonic glass made from 0.67 μm particles with polydispersity below 5% demonstrates distinct reflection peaks coming from Mie resonances of the single particles. The extinction cross section for a single sphere with diameter D = 0.67 μm and the experimental hemispherical diffuse reflection from the ceramic photonic glass made of spheres of the same diameter (L = 40 μm) are shown in Figure 7. It can be seen that a reflectivity up to 93% in visible range was achieved for 40 μm film thickness. The extinction cross section is enhanced when a Mie mode is excited in the ceramic sphere. It can be seen also from Figure 7 that we have several peaks in the range from 0.4 to 1.8 μm due to Mie resonances of the isolated ceramic spheres. The scattering is more efficient at those wavelengths, and therefore, the reflection maxima are observed. The calculated and measured peaks of the Mie resonances are in good agreement in the range of 0.4−1.2 μm, but the first Mie resonance of a single sphere at 1.47 μm moved to 1.67 μm. Mie resonances of low order have far reaching evanescent fields outside of the particle and thus are influenced by neighboring particles. In order to completely characterize this system, we show the experimental transport mean free path $l_t(\lambda)$ in a photonic glass with sphere diameter D = 0.67 μm in an inset in Figure 7. In the absence of absorption and for thickness $L \gg l_t(\lambda)$, the total transmission through the photonic glass can be calculated as[31]

$$T(\lambda, L) = \frac{l_t(\lambda) + z_e}{L + 2z_e}, \quad z_e = \frac{2}{3} l_t(\lambda) \frac{1 + R_i}{1 - R_i} \tag{4}$$

where R_i, is the integrated reflection coefficient due to the contrast between the surrounding air and the effective refractive index of the scale interface.[31] We can obtain the total transmission by $T(\lambda,L) = 1 - R(\lambda,L) - A(\lambda,L)$, where $A(\lambda,L) = 0$ due to low absorptivity of ZrO_2 for wavelengths in the visible and NIR range. The diffuse light transport through such system also has resonant behavior. Such a ceramic photonic glass is an interesting medium to investigate light propagation in resonant random media, random lasing and photonic Anderson localization due to resonant behavior of diffuse light transport through such systems. The more elaborate study of the resonant behavior of the presented photonic glass will be done in a separate work. If one reduces the particle diameters to 200−300 nm then this ceramic photonic glass can also be used for high temperature structural coloration. Such colorants do not include toxic heavy metals or transition metals, in contrast to standard high temperature stable inorganic pigments.

CONCLUSION

We reported on ceramic photonic glasses, new disordered materials obtained by sedimentation of zirconia microparticles. This novel material can be used for a wide range of applications, such as thermal radiation barrier coatings, high

dx.doi.org/10.1021/ph500224r | ACS Photonics 2014, 1, 1127−1133

temperature structural coloration, broadband visible reflectors, resonant random lasers, and photonic Anderson localization. We have studied how disordered arrays of zirconia microparticles can efficiently reflect visible and infrared electromagnetic radiation in a broad wavelength range. The hemispherical diffuse reflection from the disordered structure has broadband characteristics with a cut off defined by the sphere size. A reflectivity up to 93% in the visible range was achieved for 40 μm film thickness. Our simulations and experiments indicate that high reflection efficiencies in a wavelength range of 1−6 μm can be expected for ceramic photonic glasses with zirconia microparticles of 3 μm diameter. The calculated total heat flux transferred through a layer of ceramic photonic glass is an order of magnitude smaller heat flux compared to conventional TRBCs for a relatively thin coating of 100 μm.

METHODS

Simulations. Simulations were performed using the finite-difference time-domain method (FDTD), implemented as a freely available software package Meep,[32] with a resolution of 32 pixels per lattice spacing and subpixel smoothing of the dielectric function for more precise modeling of the finer structure features. The reflectance was calculated by modeling the propagation of an incident plane wave at normal incidence (z direction in our model). The FDTD calculation region spanned 18 μm × 18 μm size in the x−y plane, with periodic boundary conditions at the sides. Along the z-axis direction at the top and bottom of the simulation structure, perfectly matched layer boundary conditions were imposed. The thickness of the photonic glass is L along the z-axis direction. The refractive index of the ZrO_2 is assumed as n = 2.12. All calculated disordered structures possess 40% porosity. Models of random structures were obtained using event-driven molecular dynamics simulations of a monodisperse hard sphere system implemented as a freely available software package DynamO.[33] We performed numerical computations of the extinction cross section for a single ZrO_2 sphere using the finite-integration-time-domain simulation with CST Microwave Studio.

Synthesis of Zirconia Microparticles. Zirconia particles, 0.67 μm: 6.5 mL of a zirconium tetrabutoxide solution (80% in butanol, Aldrich, stored in a glovebox) were quickly injected into a rapidly agitated 200 mL solution of eicosanoic acid (1.7 mmol/L, 99%, Sigma-Aldrich) and Millipore water (0.22 mol/L) from a Millipore Simplicity System (resistivity 18.2 MΩ·cm) in anhydrous ethanol (0.01% maximum water content, VWR). The reaction was carried out at 60 °C under an inert gas atmosphere. After an induction time of 20 s, the transparent solution turned white and was gently stirred for another 4 h. After the reaction was completed, the particle suspension was cooled down and the particles were separated via centrifugation at 0 °C and washed thoroughly with ethanol.

2.1 and 2.6 μm zirconia particles: Butanol with 0.1% maximum water content was further dried over 4 Å molecular sieves and freed from dust with a 200 nm syringe filter. The reaction was carried out in a 500 mL wide-mouth glass bottle. 2.12 g eicosanoic acid were added to 200 mL of dried butanol, heated to 50 °C and stirred vigorously. After 30 min, 24.4 mL zirconium propoxide solution (70% in propanol, Acros for the 2.1 μm particles, and Alfa Aesar for the 2.6 μm particles) were added to the solution and stirred for another 30 min. A freshly prepared mixture of 174 mL of butanol and 2.8 mL of Millipore water was added to this over the course of 1 min. The concentrations of eicosanoic acid and water in the reaction solution were 18.1 mmol/L and 0.416 mol/L, respectively. After an induction time of between 20 and 40 min, the transparent solution turned white. Subsequently the stirring was stopped and the bottle was put on a tube roller (SRT6 from Stuart, roller size length × diameter: 340 × 30 mm) for an aging time of 90 min at a rotation speed of 15 rpm. After the aging time, the white suspension was quenched by pouring it into 400 mL of 0 °C cold butanol and the particles were separated by centrifugation and washed thoroughly with butanol and acetone. The particles were separated by centrifugation at 0 °C and washed thoroughly with butanol and acetone. The suspensions were precalcined in two steps with the first plateau at 120 °C and the second at 450 °C for 3 h each at a heating rate of 5 °C min^{-1}. Particles with diameters of 3.0 μm and larger could not be fabricated at a sufficiently good quality. When the aging time was prolonged to over 90 min the particles showed no substantial increase in diameter. However, a longer aging time caused the particles to agglomerate and secondary nucleation to occur. In order to be able to synthesize particles with diameters of over 3.0 μm the water content and the aging conditions will be optimized in further experiments.

Fabrication of Photonic Glass. The photonic glass films were deposited by drop casting. Suspensions were prepared by mixing the precalcined zirconia spheres with ethylene glycol at a concentration of 300 mg mL^{-1}. Mixtures were ultrasonicated for 30 min for homogenization. Suspensions were drop-cast within a silicone ring fixed to silica glass or quartz substrates. After drop-cast the substrates were heated on a hot plate at 150 °C to promote evaporation of the solvent. The resulting area of the sample was 4.5 cm^2, controlled by the diameter of the silicone ring. In order to vary the thickness of the films different amounts of suspension were drop-cast. The deposited layers were calcined at 600 °C (D = 0.67 and 2.1 μm) and 700 °C (D = 2.6 μm) at a heating rate of 5 °C min^{-1} for 2 h. Different calcination temperatures were chosen in order to ensure the elimination of organic materials present due to the synthesis process as well as the ethylene glycol.

XRD Measurements. X-ray diffraction (XRD) measurements were performed with Cu Kα radiation and a GADDS detector (D8 Discover, Bruker AXS). XRD spectra were matched with the database from Joint Committee on Powder Diffraction File (JCPDF).

Room Temperature Reflection Spectra. The hemispherical diffuse reflections of the photonic glasses between 300 nm and 2.5 μm are measured using a UV/Vis spectrometer (Lambda 1050, PerkinElmer) with integrating sphere accessory. A Fourier transform infrared (FTIR) spectrometer (Vertex 70, Bruker) with a gold-coated integrating sphere accessory is used to measure the hemispherical transmittance and reflectance in the infrared region between 2 and 6 μm.

High Temperature Reflection Spectra. The sample was placed into a high temperature heating stage (TS1500, Linkam) and the entire furnace was mounted to the microscope (Hyperion 2000, Bruker) that is coupled to the FTIR spectrometer. The sample was heated in air atmosphere at T = 900 °C for 1 h and cooled down to room temperature under vacuum (~2 × 10^{-2} mbar) in order to protect the sample from H_2O reabsorption. The reflected light from the samples was focused/collected with a 15× reflective microscope objective and the signal was measured with a liquid N_2 cooled MCT

dx.doi.org/10.1021/ph500224r | ACS Photonics 2014, 1, 1127−1133

detector. The reflectance spectrum was measured by using a gold mirror as reference.

AUTHOR INFORMATION

Corresponding Author

*E-mail: pavel.dyachenko@tuhh.de.

Author Contributions

‡These authors contributed equally to this work (J.J.d.R. and E.W.L.).

Notes

The authors declare no competing financial interest.

ACKNOWLEDGMENTS

The authors gratefully acknowledge financial support from the German Research Foundation (DFG) via SFB 986 "Tailor-Made Multi-Scale Materials Systems: M^3", Projects C2, C4, and C6. The authors also acknowledge the support from CST, Darmstadt, Germany, with their Microwave Studio software.

REFERENCES

(1) Wiersma, D. S. Disordered Photonics. *Nat. Photonics* **2013**, *7*, 188−196.

(2) Shi, L.; Zhang, Y.; Dong, B.; Zhan, T.; Liu, X.; Zi, J. Amorphous Photonic Crystals with Only Short-Range Order. *Adv. Mater.* **2013**, *25*, 5314−5320.

(3) Synnefa, A.; Santamouris, M.; Livada, I. A Study of the Thermal Performance of Reflective Coatings for the Urban Environment. *Sol. Energy* **2006**, *80*, 968−981.

(4) Mosk, A. P.; Lagendijk, A.; Lerosey, G.; Fink, M. Controlling Waves in Space and Time for Imaging and Focusing in Complex Media. *Nat. Photonics* **2012**, *6*, 283−293.

(5) Bertolotti, J.; van Putten, E. G.; Blum, C.; Lagendijk, A.; Vos, W. L.; Mosk, A. P. Noninvasive Imaging through Opaque Scattering Layers. *Nature* **2012**, *491*, 232−234.

(6) Takeoka, Y. Stimuli-Responsive Opals: Colloidal Crystals and Colloidal Amorphous Arrays for Use in Functional Structurally Colored Materials. *J. Mater. Chem. C* **2013**, *1*, 6059−6074.

(7) Clarke, D. R.; Levi, C. G. Materials Design for the Next Generation Thermal Barrier Coatings. *Annu. Rev. Mater. Res.* **2003**, *33*, 383−417.

(8) Shklover, V.; Braginsky, L.; Witz, G.; Mishrikey, M.; Hafner, C. High-Temperature Photonic Structures. Thermal Barrier Coatings, Infrared Sources and Other Applications. *J. Comput. Theor. Nanosci.* **2008**, *5*, 862−893.

(9) Van Albada, M. P.; Lagendijk, A. Observation of Weak Localization of Light in a Random Medium. *Phys. Rev. Lett.* **1985**, *55*, 2692−2695.

(10) Lawandy, N. M.; Balachandran, R. M.; Gomes, A. S. L.; Sauvain, E. Laser Action in Strongly Scattering Media. *Nature* **1994**, *368*, 436−438.

(11) Dalichaouch, R.; Armstrong, J. P.; Schultz, S.; Platzman, P. M.; McCall, S. L. Microwave Localization by Two-Dimensional Random Scattering. *Nature* **1991**, *354*, 53.

(12) García, P. D.; Sapienza, R.; Blanco, Á.; López, C. Photonic Glass: A Novel Random Material for Light. *Adv. Mater.* **2007**, *19*, 2597−2602.

(13) García, P. D.; Sapienza, R.; López, C. Photonic Glasses: A Step Beyond White Paint. *Adv. Mater.* **2010**, *22*, 12−19.

(14) Gottardo, S.; Sapienza, R.; García, P. D.; Blanco, A.; Wiersma, D. S.; López, C. Resonance-Driven Random Lasing. *Nat. Photonics* **2008**, *2*, 429−432.

(15) Kelly, M. J.; Wolfe, D. E.; Singh, J.; Eldridge, J.; Zhu, D. M.; Miller, R. Thermal Barrier Coatings Design with Increased Reflectivity and Lower Thermal Conductivity for High-Temperature Turbine Applications. *Int. J. Appl. Ceram. Technol.* **2006**, *3*, 81−93.

(16) Lee, H. S.; Kubrin, R.; Zierold, R.; Petrov, A. Yu.; Nielsch, K.; Schneider, G. A.; Eich, M. Thermal Radiation Transmission and Reflection Properties of Ceramic 3D Photonic Crystals. *J. Opt. Soc. Am. B* **2012**, *29*, 450−457.

(17) Kubrin, R.; Lee, H. S.; Zierold, R.; Petrov, A. Yu.; Janssen, R.; Nielsch, K.; Eich, M.; Schneider, G. A. Stacking of Ceramic Inverse Opals with Different Lattice Constants. *J. Am. Ceram. Soc.* **2012**, *95*, 2226−2235.

(18) Lee, H. S.; Kubrin, R.; Zierold, R.; Petrov, A. Yu.; Nielsch, K.; Schneider, G. A.; Eich, M. Photonic Properties of Titania Inverse Opal Heterostructures. *Opt. Mater. Express* **2013**, *3*, 1007−1019.

(19) Kubrin, R.; do Rosario, J. J.; Lee, H. S.; Mohanty, S.; Subrahmanyam, R. P.; Smirnova, I.; Petrov, A.; Petrov, A. Yu.; Eich, M.; Schneider, G. A. Vertical Convective Coassembly of Refractory YSZ Inverse Opals from Crystalline Nanoparticles. *ACS Appl. Mater. Interfaces* **2013**, *5*, 13146−13152.

(20) Widoniak, J.; Eiden-Assmann, S.; Maret, G. Synthesis and Characterisation of Monodisperse Zirconia Particles. *Eur. J. Inorg. Chem.* **2005**, *2005*, 3149−3155.

(21) Yan, B.; McNeff, C. V.; Carr, P. W.; McCormick, A. V. Synthesis and Characterization of Submicron-to-Micron Scale, Monodisperse, Spherical, and Nonporous Zirconia Particles. *J. Am. Ceram. Soc.* **2005**, *88*, 707−713.

(22) Takeoka, Y.; Honda, M.; Seki, T.; Ishii, M.; Nakamura, H. Structural Colored Liquid Membrane without Angle Dependence. *ACS Appl. Mater. Interfaces* **2009**, *1*, 982−986.

(23) Harun-Ur-Rashid, M.; Imran, A. B.; Seki, T.; Ishii, M.; Nakamura, H.; Takeoka, Y. Angle-Independent Structural Color in Colloidal Amorphous Arrays. *ChemPhysChem* **2010**, *11*, 579−583.

(24) Park, J.-G; Kim, S.-H.; Magkiriadou, S.; Choi, T. M.; Kim, Y.-S.; Manoharan, V. N. Full-Spectrum Photonic Pigments with Non-iridescent Structural Colors through Colloidal Assembly. *Angew. Chem.* **2014**, *126*, 2943−2947.

(25) Buxbaum, G.; Pfaff, G. *Industrial Inorganic Pigments*; John Wiley & Sons: New York, 2006.

(26) Jansen, M.; Letschert, H. P. Inorganic Yellow-Red Pigments without Toxic Metals. *Nature* **2000**, *404*, 980−982.

(27) Garcia, N.; Genack, A. Z.; Lisyansky, A. A. Measurement of the Transport Mean Free Path of Diffusing Photons. *Phys. Rev. B* **1992**, *46*, 14475−14479.

(28) Stuke, A.; Kassner, H.; Marqués, J.-L; Vassen, R.; Stöver, D.; Carius, R. Suspension and Air Plasma Sprayed Ceramic Thermal Barrier Coatings with High Infrared Reflectance. *Int. J. Appl. Ceram. Technol.* **2012**, *9*, 561−574.

(29) Gusarov, A. V.; Kovalev, E. P. Model of Thermal Conductivity in Powder Beds. *Phys. Rev. B* **2009**, *80*, 024202.

(30) Padture, N. P.; Gell, M.; Jordan, E. H. Thermal Barrier Coatings for Gas-Turbine Engine Applications. *Science* **2002**, *296*, 280−284.

(31) Burresi, M.; Cortese, L.; Pattelli, L.; Kolle, M.; Vukusic, P.; Wiersma, D. S.; Steiner, U.; Vignolini, S. Bright-White Beetle Scales Optimise Multiple Scattering of Light. *Sci. Rep.* **2014**, *4*, 6075.

(32) Oskooi, A. F.; Roundy, D.; Ibanescu, M.; Bermel, P.; Joannopoulos, J. D.; Johnson, S. G. Meep: A Flexible Free-Software Package for Electromagnetic Simulations by the FDTD Method. *Comput. Phys. Commun.* **2010**, *181*, 687−702.

(33) Bannerman, M.; Sargant, R.; Lue, L. DynamO: A Free O(N) General Event-Driven Molecular Dynamics Simulator. *J. Comput. Chem.* **2011**, *32*, 3329−3338.